Journal of Coastal Research	13	1	81–87	Fort Lauderdale, Florida	Winter 1997

Video Estimation of Foreshore Topography Using Trinocular Stereo

K. T. Holland and R. A. Holman

College of Oceanic and Atmospheric Sciences
Oregon State University
Corvallis, OR 97331, U.S.A.

ABSTRACT

HOLLAND, K.T. and HOLMAN, R.A., 1997. Video estimation of foreshore topography using trinocular stereo. *Journal of Coastal Research,* 13(1), 81–87. Fort Lauderdale (Florida), ISSN 0749-0208.

Previous researchers have shown that topographic response to swash processes is typically rapid and occasionally substantial. However, the methods used to document these fluctuations were often labor intensive and usually resulted in only a few estimates at a limited number of survey locations. We present an automated technique for the detection of small- and large-scale variations in foreshore topography that has both high spatial and temporal resolution. This technique utilizes trinocular (three view) stereogrammetry to recover topographic information from a set of synchronous, overlapping video images. The foreshore topography is mapped by following the movement of the sharply defined foamy runup edge that visibly contrasts with the darker, underlying, saturated beachface. Under field test conditions, the video method has a vertical accuracy of between 1 and 3 cm, comparable to that of traditional surveying methods and to theoretical expectations. The advantages of this new technique are that the topography estimates are extremely dense, on the order of thousands of estimates within a 100 m^2 region, that estimates can be made on a wave by wave basis, and that sampling requires minimal manpower. This method may prove useful in the study of rapid foreshore sediment transport dynamics, such as the formation of beach cusps.

ADDITIONAL INDEX WORDS: *Nearshore, swash, image processing.*

INTRODUCTION

Topographic changes in the beach region between the upper and lower limits of swash motion (termed the foreshore region) are of interest for several reasons. The general public views the foreshore as a playground where daily, seasonal or annual changes, such as beach erosion, have a profound impact, not only on recreation but also on the local economy. Scientifically, the slope of the foreshore profile (a surprisingly ill-defined quantity) is a significant parameter scaling for many nearshore dynamical processes such as the reflectivity of the beach to incident ocean waves. Furthermore, we know that foreshore topography responds to the overlying fluid processes directly and often dramatically. DUNCAN (1964) observed continual adjustment of the foreshore profile (cumulative changes of up to 46 cm) over a single tidal cycle. WADDELL (1973) documented small fluctuations (less than 5 cm) in sediment level that rapidly progressed seaward during the backwash phase of the runup. Similarly sized, but landward propagating, oscillations have also been noted (SALLENGER and RICHMOND, 1984; HOWD and HOLMAN, 1987). However, the methods used in the acquisition of these data, which include traditional surveying techniques and periodic measurement of calibrated rods, require at least two operators working continuously throughout the sampling period and are restricted to a small number of survey locations (usually less than 20). Certainly, an automated technique for the detection of small scale variations in the beach surface is desirable.

94175 received 30 March 1995; accepted in revision 15 May 1995.

Video approaches to the measurement of nearshore phenomena have been successful in the acquisition of large amounts of data with minimal use of manpower (see review by HOLMAN *et al.,* 1993). However, mapping of topography or bathymetry using video is seldom attempted, because the determination of three-dimensional (3D) information from a single two-dimensional (2D) video image is impossible without some geometric constraint on the surface of interest. For example in nearshore studies, a sufficient constraint would be that the beach foreshore is assumed to be a planar surface having a given slope and intercept, or that an identifiable beach profile is located at a known alongshore distance. Often these or similar constraints are inappropriate; yet, recovery of the three-dimensionality of a region is still possible if multiple video images are taken from different perspectives (provided that visible patterns or points on the topographic surface exist). In this situation, the 3D coordinates of any point object, a coin for example, can be determined from multiple (independent) 2D images through a transformation directly comparable to the triangulation principles used in surveying. Therefore, estimation of the positions of numerous points would in essence define a surface. Unfortunately for us, the probability of someone leaving a pocket full of change systematically dispersed along the beachface is low! To map foreshore topography, our idea was to utilize a pattern that is consistently identifiable on most beach surfaces, the runup edge. This air-water-sediment intersection is usually distinguished by a sharply defined, light-colored, foam edge that visibly contrasts with the darker, underlying, saturated, beachface. Although this edge is not a point, after digitization

it can be thought of fundamentally as an array of point objects that trace a path in space. Since this curve moves across a portion of the active beach surface during runup, it is theoretically possible to make a mapping of the beach topography for each swash cycle.

In this paper, we present a technique for estimating foreshore topography using video image processing that is inexpensive and fully automated with high spatial and temporal resolution. This technique employs trinocular (three view) stereogrammetry to recover topographic information from a set of synchronous, overlapping images. The following section describes the theory of stereogrammetry. Next, we discuss application of this theory to foreshore mapping with results from a field test and a discussion of errors. Finally, we present suggestions for improvement of this technique.

THEORY OF STEREOGRAMMETRY

The conventional stereo technique is to record multiple, intensity images of the same scene simultaneously using displaced cameras (Figure 1). The image coordinate of a point object in the scene, observed through one camera, yields an infinite number of possible object locations along the ray from the camera focal point through the image coordinate. An image coordinate from another camera corresponding to the same object defines a second ray that disambiguates the object position to a single location in space. The fundamental problem in stereo computation is matching the corresponding pixel coordinates in the multiple stereo images, or in terms of the coin analogy, distinguishing a specific coin in each view from neighboring coins. Once coordinates from each image have been "brought into correspondence", determination of three dimensional locations is straightforward and is only a function of the position and orientation of the stereo cameras (termed the extrinsic parameters) and certain physical characteristics of the lenses, cameras and image acquisition hardware (the intrinsic parameters). The relationships between these parameters are described by what is known as the camera model. For a useful review of both camera models and stereo vision, see GREWE and KAK (1994).

A camera model is a mathematical representation of the geometrical relation between the camera and the scene and of the optical projection of the image onto the camera image plane as digitized into pixel locations in the video frame buffer. The extrinsic parameters are the spatial position of the camera focal point relative to the world coordinate system, (x_c, y_c, z_c), and the camera orientation as specified by the pan (ϕ), tilt (τ), and roll (δ) angles. Intrinsic parameters commonly include the distance from the focal point to the image plane (known as the effective focal length (f)), the pixel coordinates of the center of the lens (U_o, V_o), two distortion coefficients (k1, k2) describing errors as a function of radial displacement from the optic axis, and the horizontal and vertical image scale factors (s_x, s_y). The spatial position of the camera center can be measured directly and each camera-lens combination is often calibrated in the laboratory to determine the center coordinates, the distortion coefficients, and the scale factors. The rotation angles and the focal length are obtained by solving linear equations with inputs from the other parameters and from measurements of the world and screen coordinates of at least two, but typically more than ten control points (method fully described by LIPPMANN and HOLMAN, 1989). By incorporating the intrinsic and extrinsic parameters of the camera model, the relationship between unknown object coordinates (x, y, z) and undistorted, digitizer coordinates (U, V) can be expressed in terms of eleven calibration coefficients (A to L excluding I) (following WALTON, 1981). This undistorted image to object transformation is given by the underdetermined set of equations:

$$\begin{bmatrix} (A_1 - E_1U_1) & (B_1 - F_1U_1) & (C_1 - G_1U_1) \\ (H_1 - E_1V_1) & (J_1 - F_1V_1) & (K_1 - G_1V_1) \end{bmatrix} \begin{bmatrix} x \\ y \\ z \end{bmatrix} = \begin{bmatrix} (U_1 - D_1) \\ (V_1 - L_1) \end{bmatrix} \quad (1)$$

Given image coordinates from a single camera (U_1, V_1) and its associated calibration coefficients $(A_1–L_1)$, it is not possible to determine the object coordinates without additional information about the object space. But with similar data from a distinct additional view of the same object, the Equations 1 can be repeated for each additional camera to obtain an estimated three-dimensional object location, $(\hat{x}, \hat{y}, \hat{z})$:

$$\begin{bmatrix} (A_1 - E_1U_1) & (B_1 - F_1U_1) & (C_1 - G_1U_1) \\ (H_1 - E_1V_1) & (J_1 - F_1V_1) & (K_1 - G_1V_1) \\ (A_2 - E_2U_2) & (B_2 - F_2U_2) & (C_2 - G_2U_2) \\ (H_2 - E_2V_2) & (J_2 - F_2V_2) & (K_2 - G_2V_2) \\ \cdots & \cdots & \cdots \\ \cdots & \cdots & \cdots \end{bmatrix} \begin{bmatrix} \hat{x} \\ \hat{y} \\ \hat{z} \end{bmatrix} = \begin{bmatrix} (U_1 - D_1) \\ (V_1 - L_1) \\ (U_2 - D_2) \\ (V_2 - L_2) \\ \cdots \\ \cdots \end{bmatrix} \quad (2)$$

This is an overdetermined system of equations which can be solved in a least squares sense for $(\hat{x}, \hat{y}, \hat{z})$ for every input set of corresponding image coordinates $\{(U_1, V_1), (U_2, V_2), \ldots\}$ and calculated camera coefficients $\{(A_1–L_1), (A_2–L_2), \ldots\}$.

The most problematic aspect of using a multi-dimensional image feature (such as runup edge), as opposed to a point object, is that the identification of corresponding pixels in multiple images is far from obvious. Although particular peaks and valleys in the edge are occasionally distinctive, it is usually quite difficult to visually match the majority of the edge segments, much less individual pixels. Assuming that the video images are sampled simultaneously, the search for a match of a chosen pixel in a particular image is obviously limited to the sequence of pixels defining the runup edge in each of the additional images. However, the above camera model can be used to constrain the search for matching pairs of corresponding image points by recognizing that the ray in 3D space from the camera's optical center passing through

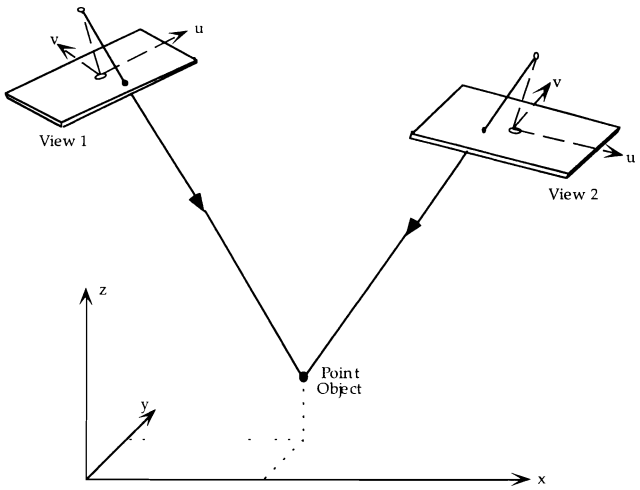

Figure 1. An example of binocular (two camera) stereometric intersection which allows the determination of the three dimensional coordinates of a point object. Known image coordinates define the location of a point object by the intersection of two rays. The focal points are indicated by the circles at the top of each focal plane.

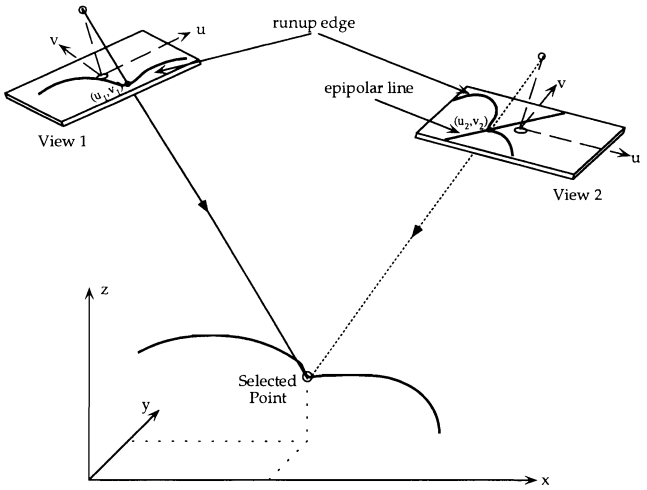

Figure 2. Stereometric intersection using the epipolar constraint. Image coordinates are selected in view 1 to determine the three dimensional coordinates of a specific point on the runup edge. The image coordinates in view 2 matching the selected coordinates are constrained to pixels corresponding to the intersection of the epipolar line and runup edge. The pair of matching coordinates is then used to estimate the location of the selected point by the intersection of the given (solid) and determined (dashed) rays. The procedure is repeated to estimate coordinates of other points along the edge.

the chosen pixel will appear as a line (referred to as the epipolar line) on the image plane of the other cameras (Figure 2). So, the search is limited to runup edge pixels that intersect the epipolar line, an enormous reduction in the number of possible matches. Unfortunately, depending upon the shape of the runup edge, multiple intersections are possible and will yield different pairs of corresponding points for a single chosen pixel in the original image. Only one of these pairs truly lies on the object surface. With two cameras, there is no simple method for eliminating this ambiguity to determine the correct pair of corresponding pixels.

Additional constraints to help distinguish the true solution from a set of possible matches can be obtained by adding a third camera (Figure 3). The basic idea is that the correct match will be restricted to edge points in the third image corresponding to the crossing of the two epipolar lines given by the other two cameras. Although there is no guarantee of a single solution, the likelihood of ambiguous matches can be minimized provided that certain geometric relationships (like near orthogonality) are maintained in the relative configuration of the cameras. In addition, since Equation 2 is overdetermined yielding a non-zero estimate of the least squares error, a certain number of the match candidates can be excluded due to improbably large errors.

FIELD EXPERIMENT

A field experiment was carried out at Gleneden Beach, Oregon between Feb. 25 and Feb. 28 1994 (in conjunction with an experiment designed to monitor swash sediment transport) to estimate spatial and temporal variability of foreshore topography. Previous studies have noted huge vertical excursions occurring at this location, up to 25 cm over a single high tide (FOX and DAVIS, 1979; BEACH and HOLMAN, 1993). A 10 by 10 m region of foreshore was selected for mapping using

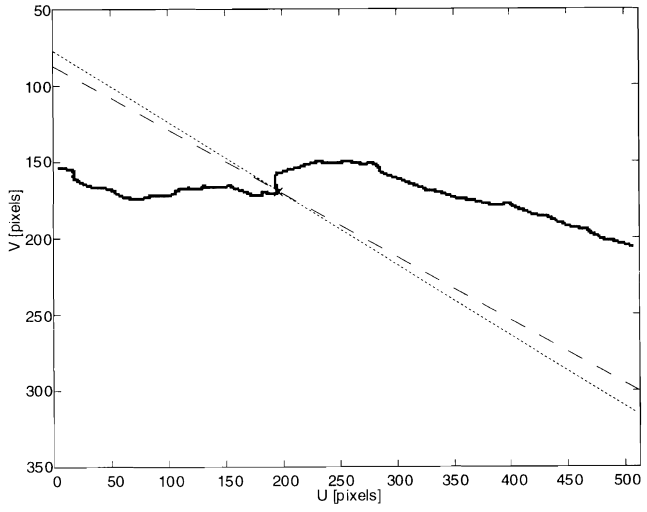

Figure 3. A video image showing application of the epipolar constraint using three cameras. The correct match is indicated by the intersection of the digitized runup edge (solid curve) and the two epipolar lines (dashed and dotted). The angle between these two lines is dependent upon the geometric relationship between the three cameras and the object location.

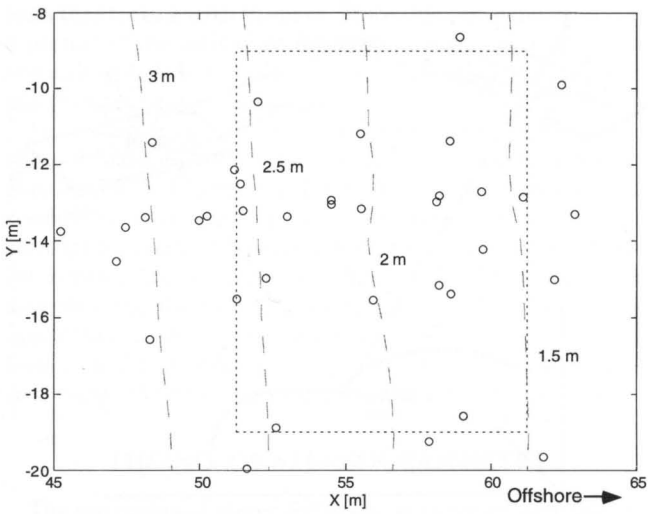

Figure 4. Foreshore elevation contours (dashed) and the enclosed study area (dotted). Circles indicate surveyed locations.

the stereo technique on the basis that it experienced an ample range of swash excursions and was in proximity to the swash sediment transport study instrumentation. The topography was relatively two-dimensional with no apparent longshore structure excepting a slight tilt in the beach surface. Groundtruth surveys of the beach surface were made at least daily using an Omni total station at a gridpoint spacing of approximately 2 m (Figure 4). Surprisingly, the survey results indicated no substantial (greater than 10 cm) changes in the foreshore topography over the four days of the experiment. For simplicity, results from the last day of the experiment (Feb. 28) will be presented as representative of the entire study.

Table 1. *Camera model parameters.*

Camera Name	N_0	x_c (m)	y_c (m)	z_c (m)	ϕ (°)	τ (°)	δ (°)	f (mm)
North	35	44.9	−25.9	8.5	42.2	65.7	−0.7	8
Mid	32	38.2	−13.7	11.7	89.7	57.6	−1.6	9
South	31	44.6	−2.1	8.6	135.7	63.4	−1.0	8

Three CCD cameras in waterproof housings were positioned overlooking the study region (Figure 5). The camera locations were surveyed relative to the same reference axes as the beach surveys. The distance from the focal points of the cameras to the center of the study region was approximately 20 m. Ground control points (GCP's), recorded during the beach surveys (a plastic ball was mounted to the survey rod), were used to calculate extrinsic and intrinsic parameters for each of the three cameras (Table 1). The field of view of the two outer cameras was 42 degrees and the view of the

Figure 5. Photograph of the field experiment showing video camera housings mounted on radio antenna towers. The circular objects on the foreshore are permanent ground control points.

Table 2. *Mean, standard deviation and maximum object space calibration error.*

Camera Name	Mean (cm)	s.d. (cm)	Max. (cm)
North	1.84	0.98	4.11
Mid	1.03	0.71	3.33
South	0.94	0.67	2.39

middle camera was 38 degrees. For all of the cameras, the horizontal and vertical footprints of a single pixel (a fundamental limit on the image resolution) were approximately 7 and 0.8 cm, respectively. The average minimum error of the camera models, as given by the magnitude of the distance of closest approach between a measured GCP in the object space and the estimated line formed by projecting the measured 2D pixel coordinates out from the image plane, was 1.3 cm. Complete statistics are provided in Table 2.

To assure that all frames were time synchronous, the video camera signals were genlocked to a common source and time stamped using both vertical interval (VITC) and longitudinal (SMPTE) time code generated from a GPS receiver. Three video cassette recorders (VCR's) were used to record the video signals onto two hour, S-VHS format, video cassettes. Following acquisition, a computer controlled, frame accurate VCR was used to locate specific frames on the tapes to be sampled using an Imaging Technology image processing system in a Sun Sparcstation 2 host. The sampling rate of the runup edges was 10 Hz and corresponds to every third frame. Image coordinates of the runup edge in each of the three views were determined using Canny edge detection with segment linking (CANNY, 1986). The trinocular epipolar constraint (see theory section) was used to match each of the pixels within a selected edge to corresponding pixel coordinates in the other two edges. Edges typically consisted of around 500 pixels. For each set of corresponding (matched) coordinates, a separate 3D runup estimate was calculated using Equation 2. Ambiguous sets containing more than three match candidates were ignored. Previous studies have shown that video identification of the runup edge is equivalent to a very near bed measurement (HOLLAND *et al.*, 1995). Therefore, by sampling of the runup edge coordinates over a half swash cycle (the uprush), a mapping of the foreshore topography in that swash region was determined. The entire analysis process was automated with no manual intervention other than to place tapes in the VCR and type a few commands at the computer keyboard. Determination of topography from 15 seconds of video input (a characteristic swash cycle length) takes the computer approximately 45 minutes and typically results in several thousand topography estimates.

RESULTS

To empirically determine the calibration accuracy of stereo triangulation using the three camera models, we input into Equation 2 sets of matching, manually digitized, image coordinates $\{(U_1, V_1), (U_2, V_2), (U_3, V_3)\}$ (determined to the nearest half pixel) corresponding to each of the GCP's used to solve the camera models. The resulting 3D position estimates

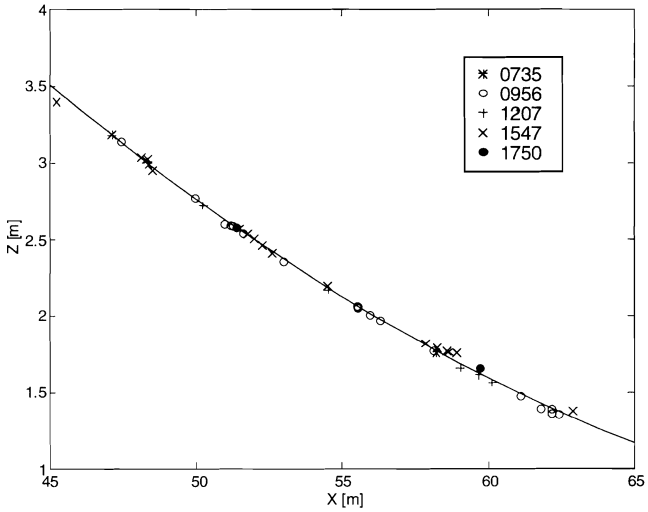

Figure 6. Comparison of survey measurements to the surface function given by Equation 3. In this diagram, the alongshore trend of the surfaces has been removed using the regression coefficient c to allow two-dimensional comparison of the observations and the best fit surface. Survey times are indicated by the various symbols. The standard deviation of the ground truth survey about the surface function was 2.2 cm. The mean and maximum absolute differences were 1.6 and 6.1 cm, respectively. Since the errors associated with the fit of this surface are close to the accuracy of our surveying method, it appears that the surface function is adequate in describing the observations.

$(\hat{x}, \hat{y}, \hat{z})$ were compared to the corresponding surveyed positions (x, y, z). The mean absolute deviation of repeated survey measurements of temporary benchmarks from their average value, indicative of the groundtruth surveying accuracy, was 1.7 cm. The mean absolute error due to triangulation, as defined by the average Euclidean distance between the estimated 3D positions and the (average) benchmark positions, was 1.9 cm, suggesting that the triangulation accuracy approximates the accuracy of traditional surveying. The maximum error was 3.5 cm.

To compare the surveyed topography with topography estimated using runup edges, the survey measurements were first fit to the surface given by the equation

$$z = ax + bx^2 + cy + d \quad (3)$$

where a, b, c and d are regression coefficient estimates. Figure 6 shows the similarity between the observed and fitted surfaces. Direct comparison of the stereo estimates and the fitted surface function is shown in Figure 7 for a single swash cycle. The difference between the stereo estimate and the fitted surface was calculated for each position estimated. Table 3 lists, for the manually digitized GCP's and for several swashes, the standard deviation of the elevations estimated using the stereo technique about the surface function given by Equation 3 along with the number of observations (N), and the mean and maximum absolute differences. Statistics obtained using surveyed GCP locations and GCP locations estimated using the stereo technique (*) are indicated. In general, the differences approach the empirical calibration ac-

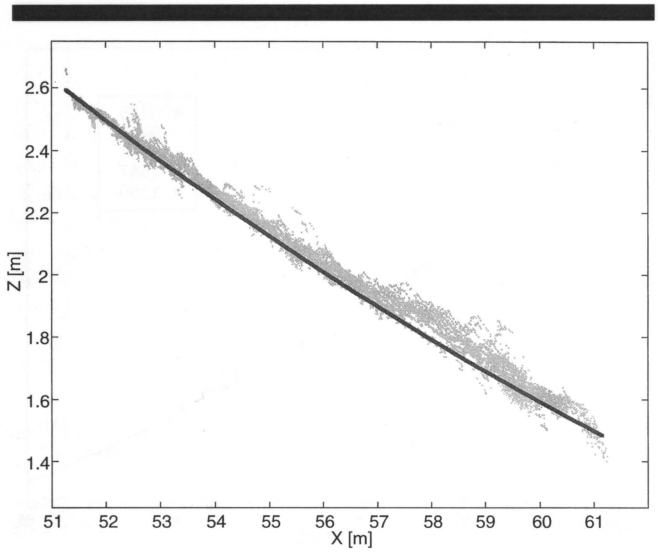

Figure 7. Comparison of stereo estimates (dots) with best fit surface (solid line). The alongshore trend of the surfaces has been removed as in Figure 6. The standard deviation of stereo elevations about the surface function was 3.8 cm. The mean and maximum absolute differences were 2.8 and 22.3 cm, respectively.

curacy of the stereo technique (1.9 cm); however on average, the stereo estimated surface lay above the ground truth surface determined from the observations. In addition, the deviations appeared to increase slightly with cross-shore distance as would be expected, since camera resolution decreases with distance from the lens.

The surveyed groundtruth within the study area were thinly scattered and the number of overlapping measurements in consecutive surveys was extremely low. Without better groundtruth, it is difficult to separate errors inherent to the stereo technique from errors introduced by small scale temporal or spatial variations of the true beach surface from the surface function or from errors resulting from inaccurate surveying. If we assume that the fitted surface perfectly represents the actual topography, then the error introduced by stereo triangulation is approximately 1.1 cm. We expect that the most logical source of additional error is in the identification of corresponding pixels using the epipolar constraint. Based on the difference between the runup edge and GCP statistics in Table 3, this additional error is between 1.4 and 1.8 cm, giving a total error of about 3 cm. Given the differences between the groundtruth and the fitted surface, it is possible that up to 2 cm of this total error is due to an imperfect fit of the function or inaccurate surveying. Therefore we conclude that the accuracy of estimation of foreshore topography using trinocular stereo with the epipolar constraint is between 1 and 3 cm.

DISCUSSION

It is clear from the results that the video method of estimating foreshore topography using trinocular stereo is at least as accurate as previously established techniques. Potential improvements to the technique are suggested by the work

Table 3. *Number of observations, standard deviation, mean absolute difference and maximum absolute difference between stereo estimates and the best fit surface for several swashes and the manually digitized ground control points (GCP's).*

Time of Swash	N	r.m.s. (cm)	Mean (cm)	Max. (cm)
12:21	7,150	3.32	2.61	23.85
12:52	5,468	3.45	2.58	17.14
12:55	5,928	3.92	2.84	23.05
13:07	17,197	3.75	2.83	22.77
13:36	6,282	3.59	2.85	19.22
Average	8,405	3.61	2.74	21.21
GCP's	16	2.23	1.55	6.13
GCP's*	16	1.82	1.09	5.50

*Indicates GCP location estimated using the stereo technique

of TSAI (1987), who bounds the error of a 3D measurement of a point object using stereo triangulation by:

$$\text{error}_{\text{total}} \leq \left[\left(1 + \frac{1}{\sqrt{6N_0N_f}}\right)\frac{z}{f} + \frac{\|T_s\|}{L\sqrt{6N_0}}\left(1 + \frac{1}{N_f}\right) + \frac{1}{2\sqrt{6N_0}} + \frac{1}{2\sqrt{6N_0}}\frac{z}{f}\right]\frac{z}{\|T_s\|}\delta + \Delta_q$$

where

- δ 2D error of the corresponding image pixel coordinates (0.025 mm or 2 pixels)
- Δq 3D error of the ground control point coordinates (assume 0)
- N_0 number of ground control points used in the calibration (40)
- N_f number of views used in triangulation (3)
- $\|T_s\|$ maximum distance between the optical centers of cameras (19 m)
- L width of the image sensor chip (6.5 mm)
- f effective focal length (8.3 mm)
- z depth of the estimate from the optical centers of the cameras (20 m)

Approximate values of the above parameters for this experiment (shown in parentheses) yield a theoretical upper error bound of 1.1 cm in accordance with our measurements that suggest an observed error of between 1 and 3 cm. To improve upon our experimental setup, the above equation suggests that one could move the cameras closer to the study area or increase the lens magnification by using a larger focal length. However, these adjustments trade off with each other if the size of the survey area is to be maintained. Since this area is not often variable, another option is to increase the separation distance between cameras. Unfortunately, this change makes pixel matching more difficult. We view the experiment setup described above as nearly optimal for our application. However, improved resolution may result from judicious placement of cameras to maximize the acute angle between epipolar lines (see Figure 3). This change would hypothetically decrease δ, the pixel matching error resulting

from the epipolar constraint and, correspondingly, decrease the total error.

The main advantage of this technique is that many thousand densely spaced samples can be made with minimal effort. In addition, the analysis process is almost completely automated, which may allow its use in longer term (months to years) studies of topographic change. One particularly intriguing investigation for which this technique is ideally suited is the documentation of beach cusp development. Beach cusps are rhythmic foreshore features, with a typical spacing between cusps of around 30 m. Models describing the processes involved in cusp development differ greatly, but generally include the interaction between the swash bore front and the underlying topography (DEAN and MAURMEYER, 1981; WERNER and FINK, 1993). The details of this interaction are poorly understood given the dearth of swash and topography observations during cusp growth. Since the stereo technique documents both the swash edge motions and the corresponding changes in topography, this method will aid our understanding of beach cusp development and foreshore sediment transport.

During this experiment, we were surprised by the stability of the foreshore as documented using the video method, with no obvious ($>$ 3 cm) erosional or accretional trends either between successive swashes or over a tidal cycle. This was unexpected given changes on the order of 10 cm documented further offshore in the surf zone and that the maximum runup velocities and swash depths (approximately 5 m/s and 10–15 cm respectively) were assumed adequate to transport sediment. We conclude that this result was not due to an error inherent to the method because the groundtruth results were similar. Instead, we suspect that the fluid and sediment processes at the site during the sampling period were in a state of equilibrium, which given the history of topographic change at that location is seldom observed.

SUMMARY

Topographic changes in the foreshore region were estimated using a video technique that utilizes trinocular (three view) stereogrammetry to recover topographic information from a set of synchronous, overlapping video images. Topography is mapped by following the movement of the sharply defined, foamy runup edge that visibly contrasts with the darker, underlying, saturated, beachface. Results from a field experiment designed to test the practicality of the technique suggest that the accuracy of the video method is between 1 and 3 cm and is comparable to that of traditional surveying methods. The advantages of this new technique are that the topography estimates are extremely dense, on the order of thousands of estimates within a 10 by 10 meter region and can be made on a wave by wave basis.

ACKNOWLEDGEMENTS

We acknowledge John Stanley for eagerly fulfilling our seemingly senseless requests concerning software and hardware details. We also thank Art Pope and his cohorts at the University of British Columbia for providing the Vista library of computational vision routines on which much of our software is based. This paper was supported by funding from the Office of Naval Research Coastal Dynamics Program (N00014-9411196) and the U.S. Geological Survey Coastal Geology Program (Cooperative agreement #1434-93-A-1124).

LITERATURE CITED

BEACH, R. and HOLMAN, R.A., 1993. Swash zone sediment transport on a steep beach. *EOS Transactions, American Geophysical Union,* 340p.

CANNY, J., 1986. A computational approach to edge detection. *IEEE Transactions on Pattern Analysis and Machine Intelligence,* PAMI 8(6), 679–698.

DEAN, R.G. and MAURMEYER, E.M., 1981. Beach cusps at Point Reyes and Drakes Bay Beaches, California, in *Proceedings of the 17th Conference on Coastal Engineering,* ASCE, Sydney, Australia, pp. 863–884.

DUNCAN, J.R., 1964. The effects of water table and tide cycle on swash-backwash sediment distribution and beach profile development. *Marine Geology,* 2, 168–187.

FOX, W.T. and DAVIS, R.A., JR., 1979. Surf zone dynamics during upwelling on the Oregon coast. *Estuarine, Coastal and Marine Science,* 9(6), 683–697.

GREWE, L.L. and KAK, A.C., 1994. Stereo Vision, in Handbook of Pattern Recognition and Image Processing: Computer Vision, vol. 2, San Diego: Academic, pp. 239–317.

HOLLAND, K.T.; RAUBENHEIMER, B.; GUZA, R.T., and HOLMAN, R.A., 1995. Runup kinematics on a natural beach. *Journal of Geophysical Research,* 100(C3), 4985–4993.

HOLMAN, R.A.; SALLENGER, A.H., JR.; LIPPMANN, T.C., and HAINES, J.W., 1993. The application of video image processing to the study of nearshore processes. *Oceanography,* 6(3), 78–85.

HOWD, P.A. and HOLMAN, R.A., 1987. A simple model of beach foreshore response to long period waves. *Marine Geology,* 78, 11–22.

LIPPMANN, T.C. and HOLMAN, R.A., 1989. Quantification of sand bar morphology: A video technique based on wave dissipation. *Journal of Geophysical Research,* 94(C1), 995–1011.

SALLENGER, A.H., JR. and RICHMOND, B.M., 1984. High-frequency sediment-level oscillations in the swash zone. *Marine Geology,* 60, 155–164.

TSAI, R.Y., 1987. A versatile camera calibration technique for high-accuracy 3D machine vision metrology using off-the-shelf TV cameras and lenses. *IEEE Journal of Robotics and Automation,* RA-3(4), 323–344.

WADDELL, E., 1973. *Dynamics of Swash and Implication to Beach Response.* Baton Rouge Technical Report #139 Louisiana State University, 47p.

WALTON, J.S., 1981. Close-range Cine-photogrammetry: A Generalized Technique for Quantifying Gross Human Motion. Ph.D. dissertation, Pennsylvania State University, 626p.

WERNER, B.T. and FINK, T.M., 1993. Beach cusps as self-organized patterns. *Science,* 260(May), 968–971.